Probing strangeness with event topology classifiers in pp collisions at the LHC with rope hadronization mechanism in PYTHIA

Suraj Prasad[1], Bhagyarathi Sahoo[1], Sushanta Tripathy[2], Neelkamal Mallick[1], and Raghunath Sahoo[1*]

[1]*Department of Physics, Indian Institute of Technology Indore, Simrol, Indore 453552, India and*

[2]*CERN, CH 1211, Geneva 23, Switzerland*

(Dated: September 10, 2024)

In relativistic heavy-ion collisions, the formation of a deconfined and thermalized state of partons, known as quark-gluon plasma, leads to enhanced production of strange hadrons in contrast to proton-proton (pp) collisions, which are taken as baseline. This observation is known as strangeness enhancement in heavy-ion collisions and is considered one of the important signatures that can signify the formation of QGP. However, in addition to strangeness enhancement, recent measurements hint at observing several heavy-ion-like features in high-multiplicity pp collisions at the LHC energies. Alternatively, event shape observables, such as charged particle multiplicity, transverse spherocity, transverse sphericity, charged particle flattenicity, and relative transverse activity classifiers, can fundamentally separate hard interaction-dominated jetty events from soft isotropic events. These features of event shape observables can probe the observed heavy-ion-like features in pp collisions with significantly reduced selection bias and can bring all collision systems on equal footing. In this article, we present an extensive summary of the strange particle ratios to pions as a function of different event classifiers using the PYTHIA 8 model with color reconnection and rope hadronization mechanisms to understand the microscopic origin of strangeness enhancement in pp collisions and also prescribe the applicability of these event classifiers in the context of strangeness enhancement. Charged-particle flattenicity is found to be most suited for the study of strangeness enhancement, and it shows a similar quantitative enhancement as seen for the analysis based on the number of multi-parton interactions.

I. INTRODUCTION

In heavy-ion collisions at the Large Hadron Collider (LHC) and Relativistic Heavy-Ion Collider (RHIC), sufficiently high energy density and temperature are reached where nuclear matter goes through a transition to the deconfined state of quarks and gluons, known as quark-gluon plasma (QGP). Enhanced production of particles with strangeness in heavy-ion collisions with respect to pp collisions, known as strangeness enhancement, is originally proposed as an indirect signature of the formation of QGP [1–3]. Also, the study of strangeness production gives an insight into quantum chromodynamics (QCD). Before the collisions, the colliding nuclear matter contained only up and down quarks, and strange quarks were not present as valence quarks. In the early state after the collision, the strange quarks are produced via hard perturbative processes via flavor creation ($q\bar{q} \rightarrow s\bar{s}$), gluon fusion ($gg \rightarrow s\bar{s}$), and flavor excitation ($gs \rightarrow gs$, $qs \rightarrow qs$). These processes are responsible for the strange particle production with higher transverse momenta after the subsequent hadronization. The non-perturbative processes dominate in the low transverse momenta for the production of strange hadrons.

In heavy-ion collisions, the abundances of strange particles relative to pions (lightest meson with up and down quarks) remain nearly constant with a change of collision centrality and collision energy [4, 5]. In elementary collisions like e^+e^- and pp collisions, based on string fragmentation models, the production of strange hadrons is significantly suppressed relative to hadrons, with only up and down quarks as strange quarks are heavier to be produced thermally ($T < m_{\rm s}$), in these hadronic and elementary collisions. Recent measurements of high multiplicity pp collisions at LHC energies have revealed that such systems exhibit features similar to heavy-ion collisions, such as long-range near-side angular correlation [6], non-zero v_2 coefficients [7], mass-ordering in hadron p_T-spectra and characterstic modifications of baryon-to-meson ratios [8], and enhanced production of muti-strange hadrons [5]. The enhanced production of strangeness with respect to pion yields which is in contrast to the traditional belief of being achievable in ultra-relativistic nucleus-nucleus collisions [5]. These measurements point towards a common underlying physics mechanism across collision systems and energies [4, 9–21]. This enhancement feature is described in the canonical thermal phase space suppression picture [22, 23]. However, other indirect signatures of QGP, such as jet quenching, have been reported to be absent in small collision systems [24]. Such behavior is quite challenging for currently popular event generators with relevant and contrasting physics models, like PYTHIA 8 and EPOS-LHC [25], to reproduce all the observed behavior simultaneously for small collision systems. Thus, the origin of the QGP-like behavior in small systems is still unclear, the microscopic origin of which is yet to be understood. Several theoretical models have been proposed to explain such behavior in small systems. One such explanation comes from the multi-parton interac-

tions (MPI)-based picture with color reconnection (CR) and ropes inherited in the PYTHIA 8 model. This model can describe some of the QGP-like behavior by including phenomenological final state hadronization mechanisms such as color reconnection [26, 27], rope hadronization (RH) [28] and string shoving [29]. However, MPI can not be accessible directly in experiments. Thus, in experiments, several measurements have been performed as a function of final state charged-particle multiplicity, which shows a significant correlation with MPI based on MC studies. However, measurements by event selections based only on mid-rapidity multiplicity have shown a stronger than linear increase of high-$p_{\rm T}$ particles in high multiplicity (HM) collisions relative to the yield in minimum-bias (MB) pp collisions [5]. This indicates a selection bias towards local fluctuations of choosing only hard pp collisions. To reduce such biases, the event selection is performed in different pseudorapidity intervals with respect to the observable of interest. However, it is found that such measurements are still biased by the hard processes at high-$p_{\rm T}$ [30]. Thus, such selection biases in measurements hinder the search for the origin of QGP-like behavior in small collision systems. To pinpoint the origin of these phenomena with significantly reduced selection bias and to bring all collision systems in equal footings, along with charged-particle multiplicity ($N_{\rm ch}$), lately several event shape observables such as transverse spherocity (S_0) [31–36] and transverse sphericity ($S_{\rm T}$) [37, 38] are inherited from the usage in e^+e^- collisions since late 1970s. Also, new types of event shape observables have been constructed such as relative transverse activity classifiers such as $R_{\rm T}$, $R_{\rm T}^{\rm min}$, and $R_{\rm T}^{\rm max}$ [40–42] and charged particle flattenicity ($\rho_{\rm ch}$) [43–45] to reduce the sensitivity to hard processes compared to the classifiers observed based only on charged-particle multiplicity. The explorations using the above-mentioned observables have been performed extensively in experiments as well as on the phenomenological front.

Various phenomenological models based on the string fragmentation process of hadronization in QCD form color ropes along with the CR mechanism qualitatively describe the strangeness enhancement at the LHC energies [28, 46, 47]. The QCD-inspired model based on Muellers's dipole formulation, called DIPSY rope [48] qualitatively describes the strangeness enhancement feature for Λ and K_S^0, while this model underestimates the production of Ω and Ξ hyperons [5]. Furthermore, a realistic MC model called HERWIG7 [49] based on the cluster mechanism of hadronization incorporates a new mechanism of color reconnection that describes the strangeness enhancement data quite well. In this model, the heavier hadrons, mostly baryons are produced geometrically and it incorporates the non-perturbative gluon splitting to produce more $s\bar{s}$ to explain the strange production. On the other hand, another cluster reconnection model was introduced which allows the reconnections between the baryonic and mesonic clusters that led to a better agreement with the data for the production of strange

baryon [50]. Recently, the effect of the range of color reconnection on strangeness enhancement is investigated in PYTHIA8 considering an MPI-based CR picture, further, a comparison of MPI-based CR and QCD-based CR is explored including color ropes [51]. Moreover, PYTHIA8 with specific tunes of RH and CR mechanism predicts the strange hadrons to pion ratios quite well as a function of charged particle multiplicity in pp collisions at $\sqrt{s} = 7$ and 13 TeV [20]. Thus, to understand the microscopic origin of strangeness enhancement in pp collisions in more detail, the study of the strangeness enhancement as a function of other existing event shape classifiers is necessary to get an insight into the applicability of event classifiers. Therefore, in the manuscript, we explore the strangeness enhancement as a function of various event shape observables such as MPI, transverse sphericity, transverse spherocity, relative transverse activity classifiers $R_{\rm T}$, and charged particle flattenicity $\rho_{\rm ch}$ using CR and RH mechanism of PYTHIA8.

In PYTHIA 8, the hadron production occurs via the incoherent break-up of the strings, which exhibit a constant energy density. This keeps the strange particle ratios the same at different multiplicity events. However, in the rope hadronization framework, color ropes are incorporated in the PYTHIA 8 model, which involves different physical processes during the hadronization process. In the RH framework, the description of the interactions among the overlapping strings is given in two steps. Firstly, it allows the nearby strings to shove each other with an interaction potential. Then, during the hadronization process, the color charges at string endpoints and in gluon kinks can act together coherently to form a rope. This leads to an increase in the effective string tension in the high-multiplicity events, which explains the strangeness enhancement feature in PYTHIA 8. This gives us an opportunity to perform the extensive study of event shape dependence of strangeness production using the tune of PYTHIA 8 with color ropes, which is the default tune for this work.

The paper is organized as follows. We start with a brief introduction in Sec. I. The discussion on the event generation methodology and definitions of event shape classifiers are given in Sec. II. The results are discussed in Sec. III and Sec. IV provides a summary and outlook of the study.

II. EVENT GENERATION AND METHODOLOGY

In this section, we discuss the event generation using the Monte Carlo event generator PYTHIA 8, specific tunes used in this study, and analysis methodology. We start the description with the pQCD-inspired PYTHIA 8 model and then discuss different event-shape observables such as charged particle multiplicity ($N_{\rm ch}$), transverse sphericity (S_T), transverse spherocity (S_0), and relative transverse activity classifier (R_T), and charged particle

Rope Hadronization	Values
Ropewalk:RopeHadronization	on
Ropewalk:doShoving	on
Ropewalk:doFlavour	on
Ropewalk:r0	0.5
Ropewalk:m0	0.2
Ropewalk:beta	1.0
Ropewalk:tInit	1.0
Ropewalk:deltat	0.05
Ropewalk:tShove	10.0

TABLE I: The parameter values of the rope hadronization model used with color reconnection mechanism.
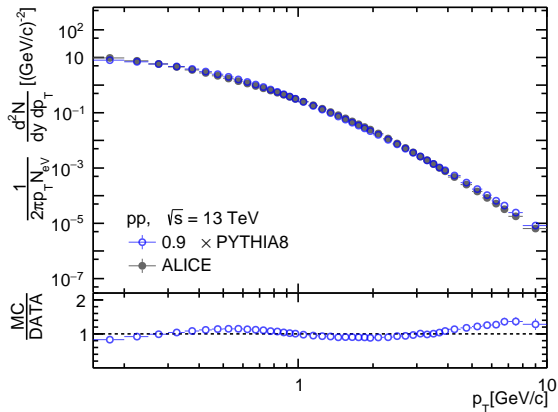

FIG. 1: Transverse momentum spectra for minimum bias pp collisions at $\sqrt{s} = 13$ TeV using PYTHIA 8 compared with the experimental measurements from ALICE [56].

flattencity (ρ_{ch}).

A. PYTHIA 8

PYTHIA is a widely used perturbative QCD-inspired Monte Carlo event generator to simulate hadronic, leptonic, and heavy-ion collisions with emphasis on physics related to small collision systems like pp collisions [52]. PYTHIA 8 involves soft and hard QCD processes and contains the libraries for initial and final state parton showers, multiple parton-parton interactions, beam remnants, string fragmentation, and particle decays. A detailed explanation of all physics processes involved in PYTHIA 8 can be found in Ref. [53].

In this study, we have used PYTHIA 8.308, an advanced version of PYTHIA 6, which incorporates the multi-partonic interactions scenario as one of the key improvements. This analysis is performed by generating 60 million events in pp collisions at $\sqrt{s} = 13$ TeV with Monash 2013 Tune (Tune:pp = 14) [54]. We

contemplate inelastic, soft QCD simulated events (Soft-QCD:inelastic=on), which allows all the single, double, and central diffractive components of the total scattering cross-section. We have considered mode 1 of color reconnection (ColourReconnection:mode = 1) along with MPI (PartonLevel:MPI = on). This newer CR scheme is combined with mode 1 of Beam Remnants (BeamRemnants:remnantMode = 1). The mode 1 of color reconnection is the QCD-based model which minimizes the string length and the color rules from QCD. As a result, the QCD multiplets can produce triplets and junctions which produce more baryons. Furthermore, along with CR, we employ another mechanism of hadronization for color strings called rope hadronization. The tunings of the rope hadronization used in this study are similar to the string-shoving mechanism introduced in PYTHIA 8. The details of the parameters used for rope hadronization are given in Table I. To set impact-parameter-plane vertices for partonic production by MPI, FSR, ISR, and beam remnants, we use the flag partonvertex (PartonVertex:setVertex = on). For the generated events, we let all the resonances decay except the ones used in our study with the switch HadronLevel:Decay = on. The particles originating from the MPIs and the beam remnants form the underlying events. The Lund-string fragmentation model performs the hadronisation of these partons [55]. The CR picture makes sure that the string between the partons is arranged in such a way that the total string length is reduced, which in turn leads to reduced particle multiplicity of the event. Here onwards in the manuscript, the mention of PYTHIA 8 would mean PYTHIA 8 Monash 2013 tune with the inclusion of color reconnection and rope hadronization mechanisms.

To check the compatibility of PYTHIA 8 with experimental data, we have compared the production cross section obtained from PYTHIA 8 as a function of transverse momentum and pseudorapidity with the ALICE experimental data [56] in pp collisions at $\sqrt{s} = 13$ TeV for all charged particles and shown in Figs. 1 and 2, respectively. As can be seen from the bottom panels, the spectral shape prediction from PYTHIA 8 is consistent with experimental data within 5%.

B. Event classifiers at the LHC

In this subsection, we define different event shape observables used at the LHC, recently.

1. Number of multi-partonic interactions (N_{mpi})

At LHC and RHIC, the hadronic collisions create a large number of particles in the final state. The basic understanding of particle production in such hadronic collisions can be made by QCD improved parton model [57]. Here, the hadrons are described as the composite of elementary particles, such as quarks and gluons, held to-
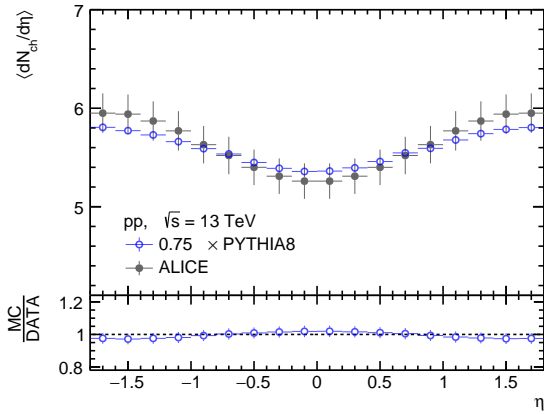
FIG. 2: Psudorapidity distribution for minimum bias pp collisions at $\sqrt{s} = 13$ TeV using PYTHIA 8 compared with the experimental measurements from ALICE [56].

gether by strong force. This composite nature of hadrons leads to the occurrence of events with multiple partonic scatterings or MPI in minimum-bias hadronic collisions. In addition to initial hard scatterings, most inelastic processes in hadronic collisions can contain several perturbatively calculable QCD interactions when one extends the pQCD theory to low p_T with some distance above Λ_{QCD} [57]. These perturbatively calculable QCD interactions, called semi-hard processes and contribute to MPI significantly, are of much importance as they can affect the final state multiplicity [57]. Thus, with an increase in the number of semi-hard processes, the number of multi-partonic interactions (N_{mpi}) rises. The events with a large N_{mpi} tend to result in large final state multiplicity and vice versa. Thus, the study of N_{mpi} is crucial for the understanding of particle production in the final state in elementary hadronic collisions.

2. Charged-particle multiplicity (N_{ch})

The charged particle multiplicity is considered as one of the most common and primary observable to disentangle the soft vs hard QCD-dominated events. Therefore, studying the observable of interest as a function of charged particle multiplicity helps us to separate these QCD processes. In general, the events with higher charged particle multiplicity specify the event to be more softer as compared to the events with lower charged-particle multiplicity. In the ALICE experiment at the LHC, the charged particle multiplicity can be measured at two different pseudorapidity regions. The Silicon Pixel Detector (SPD) and the Time Projection Chamber (TPC) measure the charged particle multiplicity at the mid-pseudorapidity region (*i.e.*, $|\eta| < 0.8$) and is denoted as N_{ch}^{mid}. On the other hand, the V0 detector with acceptance of $-3.7 < \eta < -1.7$ and $2.8 < \eta < 5.1$ measures

the charged-particle multiplicity at the forward pseudorapidity region and is denoted as N_{ch}^{fwd}.

3. Transverse sphericity (S_T)

Another interesting set of event shape observables that characterizes the underlying event (UE) shape based on the momentum of the charged hadrons is estimated from the linearized sphericity tensor [37–39];

$$S^{\mu\nu} = \frac{\sum_{i=1}^{N_{ch}} p_i^\mu p_i^\nu / |p_i|}{\sum_{i=1}^{N_{ch}} |p_i|} \quad (1)$$

where the index i runs over all the charged hadrons associated with a given event, and μ and ν indices refer to one of the (x, y, z) components of the momentum of a particle. The momentum tensor $S^{\mu\nu}$ has three eigenvalues $\lambda_1, \lambda_2, \lambda_3$. The individual eigenvalues are normalized and ordered such that $\lambda_1 > \lambda_2 > \lambda_3$ with $\lambda_1 + \lambda_2 + \lambda_3 = 1$ by definition. Using these eigenvalues, one can construct various event shape observables such that;

- Aplanarity: $A = \frac{3}{2}\lambda_3$ measures the amount of transverse momentum in or out of the plane formed by the two leading order eigenvectors and can be measured by the smallest eigenvalue λ_3. The allowed values of A lie between $0 \leq A < 1/2$, however the typical measured values lie between $0 \leq A < 0.3$. The value of A close to zero indicates the relatively planar events while the value of A close to $1/2$ indicates the isotropic events.

- Sphericity: $S = \frac{3}{2}(\lambda_2 + \lambda_3)$ measures the total transverse momentum with respect to the sphericity axis defined by the four momenta used for the event shape measurement (usually, the first eigenvector). The allowed values lie between $0 \leq S < 1$, but due to the inclusion of the smallest eigenvalue λ_3, the typical maximum value achieved in the experiment is around $S \simeq 0.8$. The value of S close to zero indicates a dijets kind of event while the value of S close to 1 indicates the isotropic events.

- $C = 3(\lambda_1\lambda_2 + \lambda_1\lambda_3 + \lambda_2\lambda_3)$ measures the events with 3 jets. The value of C tends to 0 for dijet events.

- $D = 27\lambda_1\lambda_2\lambda_3$ measures the events with 4 jets. The value of D tends to 0 for dijet or trijet events.

In hadron colliders, the event shape analysis is mostly restricted to the transverse plane to avoid the biases coming from the boost along the beam axis [38]. Therefore, similar to sphericity as defined above, another well-known event shape classifier is introduced in the transverse plane called transverse sphericity (S_T). It is one of the widely used event shape observables at Stanford Linear Accelerator Center (SLAC) to identify the existence of jets in leptonic collisions with collision energies up to

7.4 GeV [37]. Following Eq. 1, the transverse sphericity can be defined in terms of the eigenvalues of the transverse momentum matrix (S_{xy}^{Q}), given as [38]:

$$S_{xy}^{Q} = \frac{1}{\sum_i p_{T_i}} \sum_i \begin{pmatrix} p_{x_i}^2 & p_{x_i}p_{y_i} \\ p_{y_i}p_{x_i} & p_{y_i}^2 \end{pmatrix} [\text{GeV}/c]. \quad (2)$$

Here, (p_{x_i}, p_{y_i}) are the projections of transverse momentum (p_{T_i}) of ith particle in (x, y) directions. The quadratic nature of S_{xy}^{Q} in the particle momenta makes the S_{xy}^{Q} matrix to be a non-collinear safe quantity in pQCD. To make it collinear-safe, Eq. 2 can be linearized as follows,

$$S_{xy}^{L} = \frac{1}{\sum_i p_{T_i}} \sum_i \frac{1}{p_{T_i}} \begin{pmatrix} p_{x_i}^2 & p_{x_i}p_{y_i} \\ p_{y_i}p_{x_i} & p_{y_i}^2 \end{pmatrix} \quad (3)$$

Similar to sphericity, the transverse sphericity can be defined in terms of the eigenvalues of S_{xy}^{Q} matrix, i.e, λ_1, and λ_2, with $\lambda_1 > \lambda_2$, as follows.

$$S_T = \frac{2\lambda_2}{\lambda_1 + \lambda_2} \quad (4)$$

By construction, S_T ranges between 0 and 1, where $S_T \to 0$ denotes the events are jetty or pencil-like, while $S_T \to 1$ signifies the isotropic events dominated with the soft production of particles. Transverse sphericity, in this work, has been estimated in the mid-pseudorapidity region, i.e., $|\eta| < 0.8$ with charged hadrons having $p_T > 0.15$ GeV/c. For the calculation of S_T, only the events with $N_{ch}^{mid} \geq 10$ are considered.

4. Transverse spherocity (S_0)

Based on the different geometrical distributions of final state particles produced in hadronic and nuclear collisions, another event shape observable is constructed called transverse spherocity which separates the events based on their geometrical shapes. Transverse spherocity is defined as follows [31–35]

$$S_0 = \frac{\pi^2}{4} \min_{\hat{n}} \left(\frac{\sum_{i=1}^{N_{had}} |\vec{p}_{T_i} \times \hat{n}|}{\sum_{i=1}^{N_{had}} p_{T_i}} \right)^2 \quad (5)$$

Here, the unit vector $\hat{n}(n_T, 0)$ is chosen in such a way that it minimizes ratio S_0 presented within the bracket of Eq. 5. It is usually calculated using charged-particle tracks in the mid-pseudorapidity ($|\eta| < 0.8$) that have $p_T > 0.15$ GeV/c. In this study, S_0 is calculated with more than 10 charged particle tracks with $|\eta| < 0.8$ and $p_T > 0.15$ GeV/c in an event to ensure a statistically meaningful concept of topology. In Eq. 5, N_{had} refers to the total number of charged hadrons, and the multiplication factor of $\pi^2/4$ ensures that the S_0 estimator

varies from 0 to 1. The two extreme limits of spherocity correspond to the two different configurations of event topology. The value $S_0 \to 0$ corresponds to events with single back-to-back jets, while $S_0 \to 1$ corresponds to events with isotropic emission of particle production. Conventionally, the events located in the bottom 20% of the spherocity distribution are referred to as jetty events, while the top 20% of the spherocity distribution are referred to as isotropic events.

It is important to note that Eq. 5 is the p_T weighted definition of S_0 estimator. Experimentally, this weighted S_0 estimator introduces a neutral jet bias and detector smearing effect as discussed in Ref [36]. This issue could be fixed by modifying the definition via a new estimator called the unweighted transverse sphericity estimator ($S_0^{p_T=1}$). This is the unweighted transverse spherocity estimator by setting $p_T = 1$ for all the charged particles in Eq. 5. Hence, the unweighted transverse spherocity ($S_0^{p_T=1}$) is defined as follows

$$S_0^{p_T=1} = \frac{\pi^2}{4} \min_{\hat{n}} \left(\frac{\sum_{i=1}^{N_{had}} |\hat{p_T} \times \hat{n}|}{N_{had}} \right)^2. \quad (6)$$

Since the neutral jet biases were towards high-p_T particles, in Eq. 6 it is removed by setting $p_T = 1$. Furthermore, the denominator of Eq. 5, i.e., $\sum_i p_{T_i}$ is now replaced with the number of charged hadrons, i.e., N_{had}. It has been observed that with the unweighted transverse spherocity estimator the detector smearing effect is smaller than the weighted transverse spherocity estimator [36].

It is noteworthy to mention that the transverse spherocity is harder to reach the isotropic limit than for sphericity [34, 35], therefore, the discrimination power between isotropic soft events and symmetric multi-jet events might be the highest for sphericity.

5. Relative transverse activity classifier (R_T)

In recent days, a new event activity estimator has been proposed called the relative transverse activity classifier (R_T) to understand the selection bias introduced towards the hard processes, when one selects pp collisions with high event activity. This selection bias may affect the measurement and observable of interest. It is proposed that these biases can be minimized by removing the jet contribution from the event activity estimator, which can be achieved by identifying an axis that allows for the event-by-event separation of the jet contribution from the UE. In this study, the direction of the leading charged particle with the highest transverse momentum (trigger particle) is used as a reference axis to build the particle correlation with the associated particles in azimuthal angle $\Delta\phi = \phi^{trig} - \phi^{asso}$.

Thus, to separate the events based on the contribution

of jets from the UE, different topological regions are defined namely called towards, transverse, and away regions. The towards region consists of the tracks with an azimuthal angle less than $\pi/3$ relative to the trigger particle, *i.e.*, $|\Delta\phi| < \pi/3$, while the away region contains all the tracks with relative azimuthal angle $|\Delta\phi| \geq 3\pi/2$. Furthermore, the transverse region is defined to be the relative azimuthal angle within $\pi/3 \leq |\Delta\phi| < 3\pi/2$. The towards and the away regions have the largest contribution from the fragmentation of jets originating from the hardest partonic interactions in an event and are expected to be insensitive to the softer UE. However, the transverse region is perpendicular to the leading jet axis, it is expected to have the least contribution from the jet and must be dominated by the UE activity, thus a better region to build the event activity classifier R_T.

Therefore, to estimate the value of R_T, one needs the number of charged hadrons in the transverse regions (N_{ch}^T) per event and the average charged-particle multiplicity analyzed in the whole sample ($\langle N_{ch}^T \rangle$). Mathematically, the value of R_T is defined as follows;

$$R_T = \frac{N_{ch}^T}{\langle N_{ch}^T \rangle} \tag{7}$$

In Eq. 7, the angular bracket represents the event-average value of the observables. R_T is measured using the charged hadrons at $|\eta| < 0.8$. For the estimation of R_T, only the events having leading $p_T \geq 5$ GeV/c at $|\eta| < 0.8$ are considered. Here, a large value of R_T implies events dominated with the underlying event activity in contrast to a smaller value of R_T.

6. Charged-particle flattenicity (ρ_{ch})

For isotropic events, a near uniform distribution of transverse momentum is expected throughout the $\eta - \phi$ phase space. To measure the uniformity of transverse momentum distribution event-by-event, the $\eta - \phi$ region can be divided into (10×10) grid. Thus, by measuring the transverse momentum in each cell (p_T^{cell}), one can define the charged particle flattenicity (ρ_{ch}) as follows [43],

$$\rho_{ch} = \frac{\sigma_{p_T^{cell}}}{\langle p_T^{cell} \rangle} \tag{8}$$

where, $\langle p_T^{cell} \rangle$ denotes the mean and $\sigma_{p_T^{cell}}$ standard deviation of the transverse momentum distribution.

Furthermore, Eq. 8, can be written as

$$\rho_{ch} = \frac{\sqrt{\sum_i (p_T^{cell,i} - \langle p_T^{cell} \rangle)^2 / N_{cell}}}{\langle p_T^{cell} \rangle} \tag{9}$$

Keeping the ALICE 3 tracking and particle identification (PID) capabilities in mind, the charged particles in $|\eta| < 4.0$ and $p_T > 0.15$ GeV/c are considered for the estimation of $\langle p_T^{cell} \rangle$ and $\sigma_{p_T^{cell}}$. It is expected that events with jet signals along with underlying event activity have a larger spread along with the higher $\sigma_{p_T^{cell}}$. On the other hand, events having only soft production of particles will have lower spread in p_T^{cell}, and corresponding $\sigma_{p_T^{cell}}$ will be lower. Thus, the value of ρ_{ch} is expected to be smaller for isotropic events, while a large value for jetty events.

However, the current detector capabilities for PID and tracking at ALICE at the LHC and STAR at the RHIC experiments are limited to central rapidity region $|\eta| < 1.0$. Thus, using the above definition of charged-particle flattenicity defined in Eq. 9, one can not estimate the value of ρ_{ch} at the experiments. Furthermore, the measurement of both the event shape and the particle of interest in the same pseudorapidity region creates a bias. This bias can be minimized by choosing the event shape estimator in the forward rapidity region, which is in the different pseudorapidity region compared to the particle of interest [20]. Most of the present detectors can measure the charged particle multiplicity in the forward pseudorapidity. Therefore, to measure the charged particle flattenicity with the current detector scenarios, a redefinition of flattenicity is required, which is redefined in Ref. [45]. According to the new definition of charged particle flattenicity, ρ_{ch} can be estimated using the following equation.

$$\rho_{ch} = \frac{\sqrt{\sum_i (N_{ch}^{cell,i} - \langle N_{ch}^{cell} \rangle)^2 / N_{cell}^2}}{\langle N_{ch}^{cell} \rangle} \tag{10}$$

In this definition, the charged particle multiplicity is measured at the forward rapidity instead of the transverse momentum of the particles. To calculate ρ_{ch}, the $(\eta - \phi)$ phase space is divided into (8×8) cells. The average charged particle multiplicity in each cell 'i' ($N_{ch}^{cell,i}$) and the average of $N_{ch}^{cell,i}$ ($\langle N_{ch}^{cell} \rangle$) in an event is required to evalute ρ_{ch}. Similar to other standard event activity, by construction, ρ_{ch} ranges from 0 to 1 [45]. The lower limit of 0 indicates isotropic events while 1 indicates jetty events. To be consistent with other event-shape observables (e.g, sphericity, spherocity, etc.), here, throughout the manuscript, we use $1 - \rho_{ch}$ instead of ρ_{ch}. The events with $1 - \rho_{ch} \rightarrow 1$ are likely to be isotropic while events with $1 - \rho_{ch} \rightarrow 0$ exhibit jetty topology.

Table II shows the selection cuts used in this study for different event classifiers in pp collisions at $\sqrt{s} = 13$ TeV using PYTHIA 8.

III. RESULTS AND DISCUSSIONS

In this section, we explore the event shape observable dependence of particle production of primary strange (K_S^0, Λ, $\bar{\Lambda}$) and multi-strange (Ξ^+, Ξ^-, Ω^+, Ω^-) hadrons in pp collisions at $\sqrt{s} = 13$ TeV using PYTHIA 8 with

TABLE II: Selection cuts in terms of percentiles for different event classifiers in pp collisions at $\sqrt{s} = 13$ TeV using PYTHIA 8 with CR and RH mechanisms.

Percentile	N_{mpi}	$N_{\mathrm{ch}}^{\mathrm{mid}}$	$N_{\mathrm{ch}}^{\mathrm{fwd}}$	S_{T}	S_0	$S_0^{p_{\mathrm{T}}=1}$	$N_{\mathrm{ch}}^{\mathrm{T}}$	$1-\rho_{\mathrm{ch}}$
0 - 0.1	23 - 35	54 - 150	120 - 250	0.98 - 1	0.92 - 1	0.94 - 1	26 - 60	0.91 - 1
0.1 - 1	18 - 23	40 - 54	96 - 120	0.96 - 0.98	0.88 - 0.92	0.91 - 0.94	20 - 26	0.90 - 0.91
1 - 5	14 - 18	29 - 40	74 - 96	0.91 - 0.96	0.82 - 0.88	0.87 - 0.91	15 - 20	0.88 - 0.90
5 - 10	11 - 14	23 - 29	62 - 74	0.88 - 0.91	0.78 - 0.82	0.84 - 0.87	13 - 15	0.87 - 0.88
10 - 20	8 - 11	17 - 23	47 - 62	0.82 - 0.88	0.72 - 0.78	0.79 - 0.84	10 - 13	0.85 - 0.87
20 - 30	5 - 8	13 - 17	37 - 47	0.78 - 0.82	0.67 - 0.72	0.75 - 0.79	9 - 10	0.83 - 0.85
30 - 40	4 - 5	10 - 13	30 - 37	0.73 - 0.78	0.62 - 0.67	0.72 - 0.75	7 - 9	0.81 - 0.83
40 - 50	3 - 4	8 - 10	24 - 30	0.68 - 0.73	0.56 - 0.62	0.68 - 0.72	6 - 7	0.79 - 0.81
50 - 70	2 - 3	5 - 8	16 - 24	0.59 - 0.68	0.46 - 0.56	0.59 - 0.68	4 - 6	0.74 - 0.79
70 - 100	0 - 2	1 - 5	1 - 16	0 - 0.59	0 - 0.46	0 - 0.59	0 - 4	0 - 0.74

the mechanisms of color reconnection and ropes. As discussed in the previous sections, the charged-particle multiplicity serves as a probe to disentangle the hard and soft events. However, multiplicity selection is prone to selection bias. This motivates us to study the strange to non-strange ratio as a function of other event shape classifiers such as the number of multi-partonic interactions, transverse sphericity, transverse spherocity, relative transverse activity classifier, and charged-particle flattenicity. Here, we, mainly investigate $2K_S^0/(\pi^+ + \pi^-)$, $(\Lambda + \bar{\Lambda})/(\pi^+ + \pi^-)$, $(\Xi^+ + \Xi^-)/(\pi^+ + \pi^-)$, $2\phi/(\pi^+ + \pi^-)$, and $(\Omega^+ + \Omega^-)/(\pi^+ + \pi^-)$ ratios as a function of different event shape observables. For simplicity now onwards we refer these ratios as K_S^0/π, Λ/π, Ξ/π, ϕ/π, and Ω/π respectively.

We begin by comparing the results of the PYTHIA 8 model with CR and RH mechanisms for strange and multi-strange particle production yield ratio to charged pions with the ALICE results. Figure 3 shows the p_{T}-integrated yield ratios to pions $(\pi^+ + \pi^-)$ obtained in $|y| < 0.5$ as a function of mean charged particle multiplicity ($\langle dN_{\mathrm{ch}}/d\eta \rangle$) obtained at $|\eta| < 0.5$ in pp collisions at $\sqrt{s} = 13$ TeV using PYTHIA 8. Here, $\langle dN_{\mathrm{ch}}/d\eta \rangle$ is obtained for different event classes defined based on $N_{\mathrm{ch}}^{\mathrm{fwd}}$. From the figure, it is evident that the strange particle yield ratio to pions increases with an increase in $\langle dN_{\mathrm{ch}}/d\eta \rangle$. The yield ratio becomes largely prominent for particles having larger valence strange quarks. Here, K_S^0/π remains almost independent with an increase in charged particle multiplicity; however, the dependence grows when one moves from Λ/π to Ξ/π and Ω/π, which have one, two and three valence strange quarks, respectively. The results from PYTHIA 8 with rope hadronization and colour reconnection have both quantitative and qualitative agreement with the ALICE results. Figure 4 shows the strange and multi-strange particle yield ratios to pions normalized to the value obtained for the minimum bias events as a function of $\langle dN_{\mathrm{ch}}/d\eta \rangle$ in pp collisions at $\sqrt{s} = 13$ TeV using PYTHIA 8. Here, the
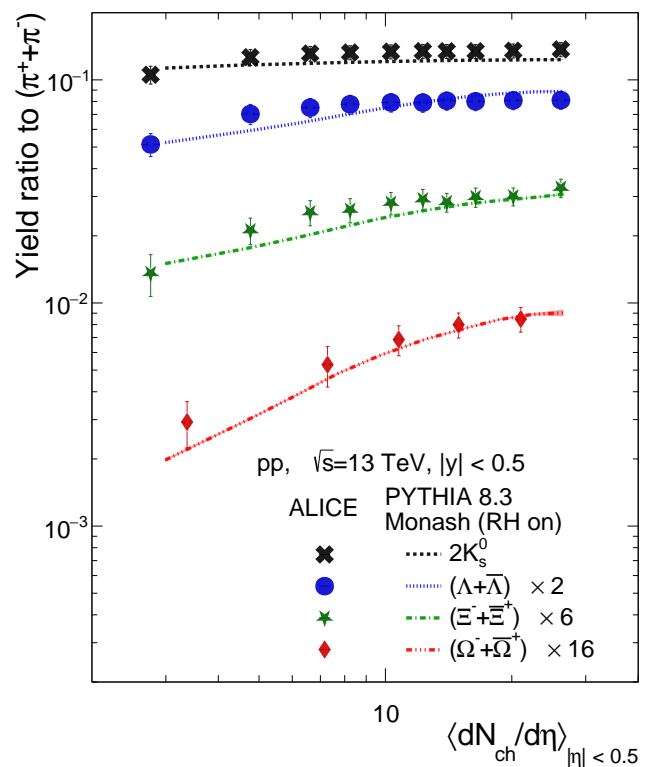

FIG. 3: p_{T}-integrated yield ratios to pions $(\pi^+ + \pi^-)$ obtained in $|y| < 0.5$ as a function of mean charged particle multiplicity ($\langle dN_{\mathrm{ch}}/d\eta \rangle$) obtained at $|\eta| < 0.5$ in pp collisions at $\sqrt{s} = 13$ TeV using PYTHIA 8, and compared with similar measurements at ALICE [21].

effect of strangeness enhancement in high multiplicity pp collisions with respect to the average minimum-bias events is visible. Again, the hardons, which have a larger number of strange quarks, show an increasing trend with a higher slope, whereas, for K_S^0, the increasing slope is
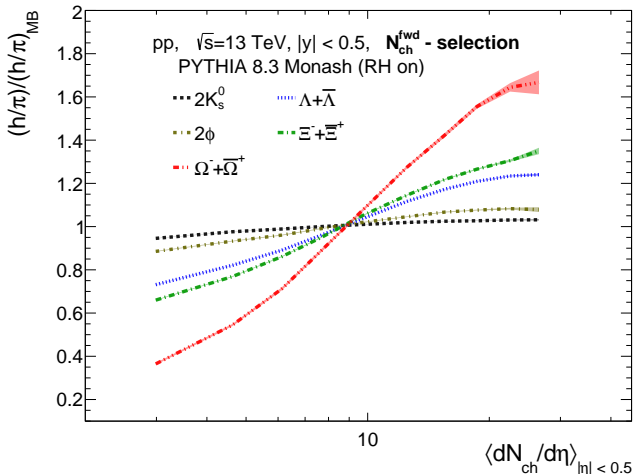
FIG. 4: Particle yield ratios to pions normalized to the values obtained for the minimum bias events as a function of $\langle dN_{ch}/d\eta \rangle$ for different classes of N_{ch}^{fwd} in pp collisions at $\sqrt{s} = 13$ TeV using PYTHIA 8.

nearly zero. This observation is consistent with the experimental measurements with ALICE for pp collisions at $\sqrt{s} = 7$ TeV [5]. However, ϕ meson with zero net strange quantum number shows a stronger enhancement trend as compared to K_S^0 having one strange quark, which can make strangeness enhancement study through ϕ meson as a function of various event shapes interesting in small systems.

After showing the feasibility of the PYTHIA 8 model with CR and RH mechanisms, let us now study strange hadron production as a function of the number of multi-parton interactions (N_{mpi}). The top panel of Fig. 5 shows the role of MPI in the production of strange hadrons having different numbers of valence strange quarks with respect to pions. Here, p_T-integrated yield ratios of strange and multi-strange hadrons to pions are shown as a function of N_{mpi} in pp collisions at $\sqrt{s} = 13$ TeV using PYTHIA 8. As one would expect, MPI plays a pivotal role in particle production, and it is also observed for strange and multi-strange hadrons. Here, the production of strange hadrons such as K_S^0, Λ, ϕ, Ξ, and Ω particles increases with respect to that of pions as one goes from events having lower value of N_{mpi} to a large N_{mpi} events. However, the yield ratios to pions seem to saturate towards higher values of N_{mpi}. The effects of RH are further enhanced in the events having a large N_{mpi} value. A large value of N_{mpi} implies a larger number of color rope formations leading to enhanced production of strange and multi-strange baryons. However, K_S^0/π and ϕ/π show negligible dependence on N_{mpi}.

In the bottom panel of Fig. 5, we show the strange and multi-strange hadron yield ratios to pions scaled to the values obtained for the minimum bias events as a function of $\langle dN_{ch}/d\eta \rangle$ for different classes of N_{mpi} in pp
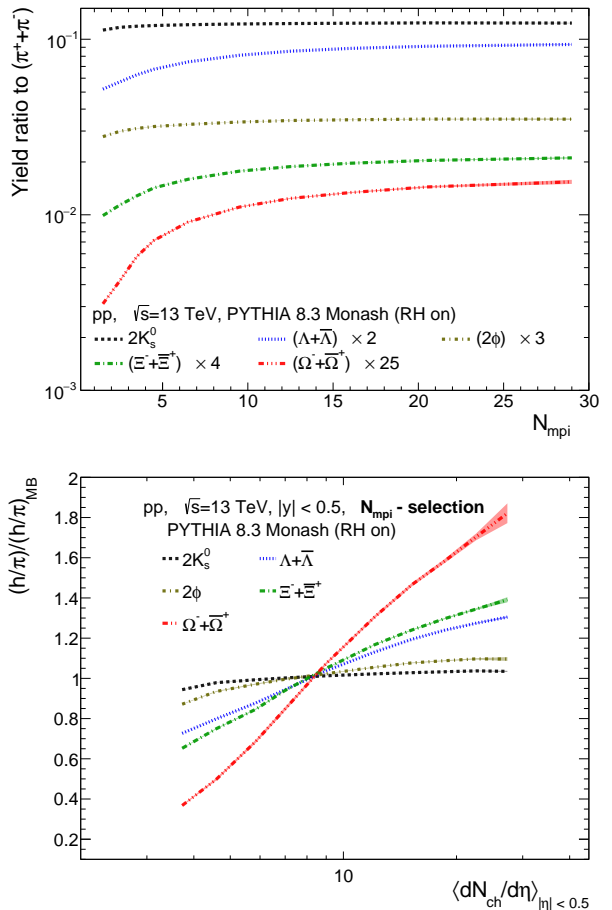

FIG. 5: Top: p_T-integrated yield ratios to pions ($\pi^+ + \pi^-$) obtained in $|y| < 0.5$ as a function of number of multi-partonic interactions (N_{mpi}) in pp collisions at $\sqrt{s} = 13$ TeV using PYTHIA 8. Bottom: Particle yield ratios to pions normalized to the values obtained for the minimum bias events as a function of $\langle dN_{ch}/d\eta \rangle$ in different classes of N_{mpi} in pp collisions at $\sqrt{s} = 13$ TeV using PYTHIA 8.

collisions at $\sqrt{s} = 13$ TeV using PYTHIA 8. Due to a positive correlation of particle multiplicity and N_{mpi}, low N_{mpi} corresponds to small $\langle dN_{ch}/d\eta \rangle$ and events having a large value of N_{mpi} leads to a large $\langle dN_{ch}/d\eta \rangle$. The strange and multi-strange hadrons show a linear increase with the increase in $\log(\langle dN_{ch}/d\eta \rangle)$ with events selected based on N_{mpi}. The effects of RH are observed to be different for strange baryons (Λ, Ξ, and Ω) from the strange meson (K_S^0) and hidden strange meson (ϕ). Interestingly, Ω, having three valence strange quarks, shows the largest enhancement with an increase in N_{mpi} in comparison to Λ, having only one valence strange quark. In contrast, the enhancement is negligible for K_s^0. Furthermore, the hidden strange meson, ϕ, shows a small dependence on the event selection based on N_{mpi}, similar to Fig. 4. Although, in experiments, the estimation of N_{mpi} is not possible, in this study, we try to probe the similar en-
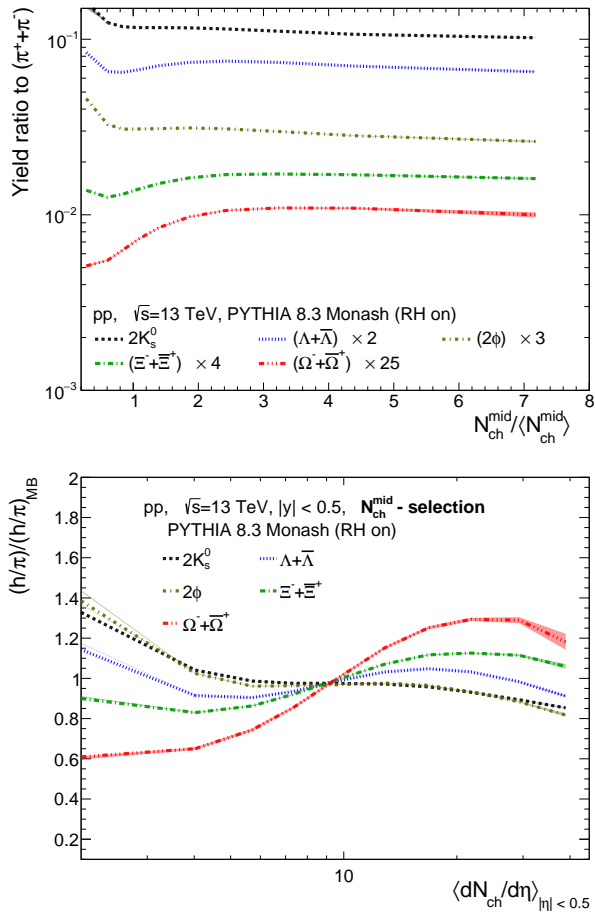
FIG. 6: p_{T}-integrated yield ratios to pions $(\pi^+ + \pi^-)$ obtained in $|y| < 0.5$ as a function of charged particle multiplicity obtained in the mid-pseudorapidity $(N_{\mathrm{ch}}^{\mathrm{mid}})$ (top) and forward pseudorapidity $(N_{\mathrm{ch}}^{\mathrm{fwd}})$ (bottom) in pp collisions at $\sqrt{s} = 13$ TeV using PYTHIA 8.

hancement of different strange hadron production using different event shapes.

The top panel of Fig. 6 shows the p-integrated yield ratios of strange hadrons to pions as a function of charged-particle multiplicity obtained in the mid-pseudorapidity $(N_{\mathrm{ch}}^{\mathrm{mid}})$ regions in pp collisions at $\sqrt{s} = 13$ TeV using PYTHIA 8. Similar to Figs. 3 and 5, strangeness enhancement is found to be proportional to the strangeness content of the hadrons. In addition, the bottom panel of Fig. 6 indicates a decrease in the strange to non-strange ratios in the high multiplicity pp collisions. This behavior is not present when one studies the strangeness as a function of MPI and forward-rapidity multiplicity selection. This could be due to the auto-correlation bias introduced while selecting charged-particle multiplicity in the mid-pseudorapidity region as the particle of interest is also studied in the mid-rapidity region. This autocorrelation bias, where events are selected based on the charged particle multiplicity, which is mostly pions, causes the ratio

to the neutral particle to pions, such as K_S^0/π, ϕ/π decrease as the particle multiplicity increases. However, for the neutral strange baryon, Λ, the self-normalised yield ratio slightly increases in $7 \lesssim \langle dN_{\mathrm{ch}}/d\eta \rangle \lesssim 15$, followed by a decrease in the lower and high $\langle dN_{\mathrm{ch}}/d\eta \rangle$ regions, which can be attributed to the competing effects of RH and autocorrelation bias due to event selection. This effect is negligible for the charged hadron ratios to pions, such as Ξ/π and Ω/π, which increase with increased charged-particle multiplicity except for the highest multiplicity class. In addition, due to this auto-correlation bias, the linear increment of the yield ratios scaled to the MB events with increasing $\log(\langle dN_{\mathrm{ch}}/d\eta \rangle)$ is absent when the events are selected based on the charged particle multiplicity at the midrapidity. Therefore, it can be inferred that the event selection in different charged-particle multiplicity windows plays an important role in describing the dynamics of the strange hadron production. Furthermore, the relative production of the hidden strange ϕ particle slightly decreases with $N_{\mathrm{ch}}^{\mathrm{mid}}$, similar to the production of K_S^0. This implies that due to the auto-correlation bias of event selection, the neutral mesons behave similarly irrespective of their valence strange quark content.

The top panels of Figs. 7 and 8 show the integrated yield ratios of strange and multi-strange hadrons to pions as a function of p_{T}−weighted transverse spherocity (S_0) and unweighted transverse spherocity $(S_0^{p_{\mathrm{T}}=1})$ in pp collisions at $\sqrt{s} = 13$ TeV using PYTHIA 8, respectively. As discussed in the previous section, experimentally, the original p_{T}−weighted S_0 estimator introduces a neutral jet bias and detector smearing effect, reported in Ref [36]. This issue could be fixed by modifying the definition via a new estimator called p_{T}-unweighted transverse spherocity estimator $(S_0^{p_{\mathrm{T}}=1})$. It is observed that the K_S^0/π, Λ/π, Ξ/π, and ϕ/π ratios remains almost constant with S_0 and $S_0^{p_{\mathrm{T}}=1}$. In contrast, Ω/π shows dependence on both S_0 and $S_0^{p_{\mathrm{T}}=1}$, which increases around 15% from lowest to highest classes of transverse spherocity. It is important to note that, here, the yield ratios to pions are comparable to the values in high multiplicity events as observed in Figs. 5, and 6. This is the consequence of event selection cut of $N_{\mathrm{ch}}^{\mathrm{mid}} \geq 10$ which is applied during the definitions of S_0 and $S_0^{p_{\mathrm{T}}=1}$.

The bottom panel of Figs. 7 and 8 show self normalized yield ratios of the strange and multi-strange particle to pions as a function of $\langle dN_{\mathrm{ch}}/d\eta \rangle$ obtained in the different classes of S_0 and $S_0^{p_{\mathrm{T}}=1}$ in pp collisions at $\sqrt{s} = 13$ TeV using PYTHIA 8. Here, $\langle dN_{\mathrm{ch}}/d\eta \rangle$ for the highest and lowest classes of S_0 and $S_0^{p_{\mathrm{T}}=1}$ range only between 10 to 20, which is very limited in comparison to event selection with $N_{\mathrm{ch}}^{\mathrm{fwd}}$ or N_{mpi}. This indicates a weaker correlation of transverse spherocity with $dN_{\mathrm{ch}}/d\eta$ as compared to the correlation of $dN_{\mathrm{ch}}/d\eta$ with $N_{\mathrm{ch}}^{\mathrm{fwd}}$ or N_{mpi}. However, $S_0^{p_{\mathrm{T}}=1}$ covers a slightly broader range of $\langle dN_{\mathrm{ch}}/d\eta \rangle$ region as compared to S_0. For Ω particle, the double ratio has a steeper increase with $\langle dN_{\mathrm{ch}}/d\eta \rangle$, when
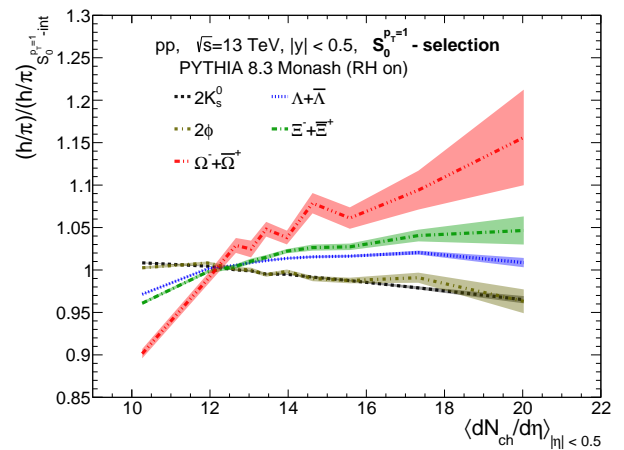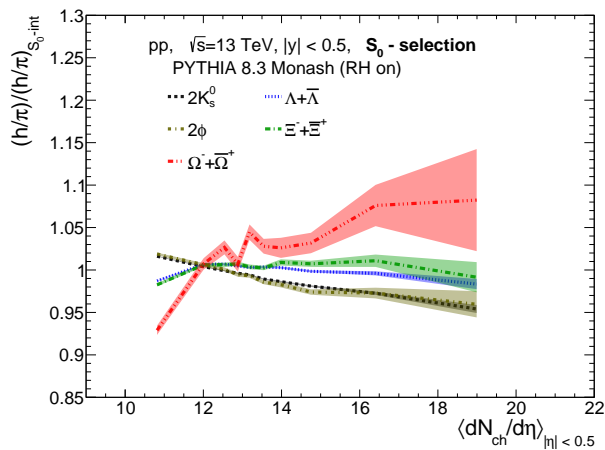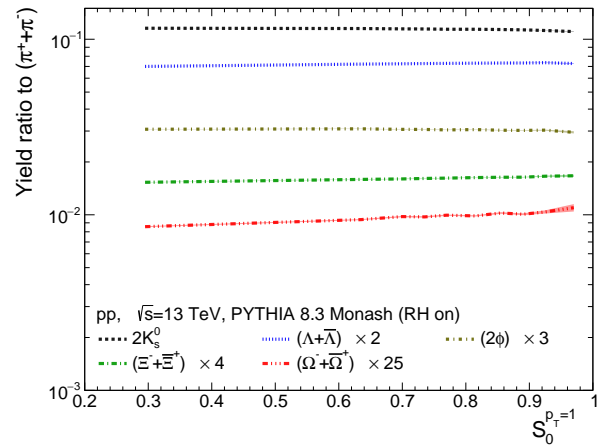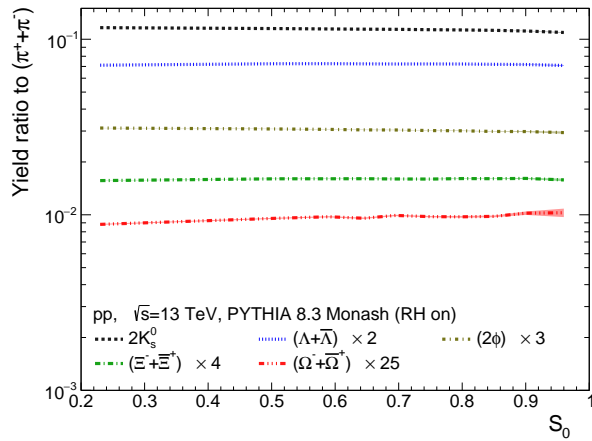
FIG. 7: p_T-integrated yield ratios to pions as a function of p_T−weighted transverse spherocity (S_0) (top) and particle yield ratios to pions normalized to the values obtained for the spherocity integrated events (bottom) for $|y| < 0.5$ in pp collisions at $\sqrt{s} = 13$ TeV using PYTHIA 8.

FIG. 8: p_T-integrated yield ratios to pions as a function of p_T−unweighted transverse spherocity (S_0) (top) and particle yield ratios to pions normalized to the values obtained for the spherocity integrated events (bottom) for $|y| < 0.5$ in pp collisions at $\sqrt{s} = 13$ TeV using PYTHIA 8.

the events are selected with $S_0^{p_\text{T}=1}$ as compared to S_0. For Ξ and Λ, S_0 provides similar double ratio values while a distinction is observed for the $S_0^{p_\text{T}=1}$ case. Here, for $S_0^{p_\text{T}=1}$, the ratio for Ξ increases rapidly in comparison to Λ with the increase in $\langle dN_\text{ch}/d\eta \rangle$, holding onto the scaling of the strangeness quantum number of strange baryons. Furthermore, for ϕ and K_0^S, one finds that the double ratios decrease with increase in $\langle dN_\text{ch}/d\eta \rangle$ for both S_0 and $S_0^{p_\text{T}=1}$ cases. However, the rate of decrease of the slope is larger for S_0 case as compared to $S_0^{p_\text{T}=1}$. These trends for ϕ and K_0^S are believed to be a consequence of measuring spherocity and the particles in overlapping rapidity regions, which is absent when event shapes are obtained in different rapidity regions, for example in Figs. 4 and 5. Thus, we may conclude that, for the study of strangeness production in pp collisions, $S_0^{p_\text{T}=1}$ possess a small selection bias but a better observable as compared to S_0 with wider multiplicity coverage.

Figure 9 shows the p_T-integrated yield ratios to pi-

ons normalized to spherocity-integrated events for top 1% events as a function of $S_0^{p_\text{T}=1}$ in pp collisions at $\sqrt{s} = 13$ TeV using PYTHIA 8, and is compared with the corresponding experimental measurements at ALICE [36]. It is observed that both the model predictions and experimental measurements agree with each other and do not show significant dependence on the strangeness content of the particle.

The top panel of Fig. 10 shows the p_T-integrated yield ratios of strange and multi-strange hadrons to pions as a function of transverse spherocity in pp collisions at $\sqrt{s} = 13$ TeV using PYTHIA 8. Similar to Fig. 7, one finds negligible dependence of K_S^0/π, Λ/π, Ξ/π, ϕ/π, and Ω/π on transverse spherocity (S_T). So, in conclusion, we found that events with isotropic emission of particles have almost similar behavior of strange to non-strange ratios to events dominated by jets when we choose events having $N_\text{ch}^\text{mid} \geq 10$. Therefore, the transverse spherocity, weighted and unweighted transverse spherocity event
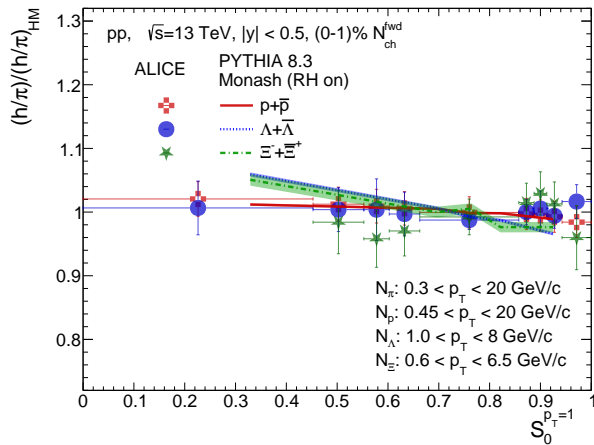
FIG. 9: Particle yield ratios to pions normalized to the values obtained for the sphericity integrated events for top 1% $N_{\text{ch}}^{\text{fwd}}$ events as a function of $S_0^{p_{\text{T}}=1}$ in pp collisions at $\sqrt{s} = 13$ TeV using PYTHIA 8. The model predictions are compared with the corresponding experimental data with ALICE [36].

classifiers are inadequate to study the strangeness suppression characteristics in low-multiplicity pp collisions using the PYTHIA 8 model; however, their applicability in the highest multiplicity classes is worth investigating.

The bottom panel of Fig. 10 shows strange and multi-strange hadron yield ratios to pions scaled to the values obtained in the sphericity integrated events as a function of $\langle dN_{\text{ch}}/d\eta \rangle$ obtained in different classes of S_{T} in pp collisions at $\sqrt{s} = 13$ TeV using PYTHIA 8. Intriguingly, S_{T} probes even smaller range of $\langle dN_{\text{ch}}/d\eta \rangle$ as compared to S_0 or $S_0^{p_{\text{T}}=1}$, indicating a small correlation between S_{T} and particle multiplicity. Furthermore, similar to S_0 in Fig. 8, one finds similar enhancement trends for Ω, Ξ, and Λ baryons and a suppression trends for ϕ, and K_0^S mesons with an increase in $\langle dN_{\text{ch}}/d\eta \rangle$ obtained in different classes of S_{T}. Notably, the amplitudes for these enhancement or suppression trends using S_{T} are the smallest compared to other event shapes.

In the top panels of Fig. 11 show the K_S^0/π, Λ/π, Ξ/π, ϕ/π, and Ω/π ratios as a function of R_{T} in toward (left) and transverse (right) regions of pp collisions at $\sqrt{s} = 13$ TeV using PYTHIA 8. Here we have restricted the strange hadrons $p_{\text{T}} < 5$ GeV/c to avoid the bias caused by the trigger particle selection for R_{T} [41, 42]. It is observed that the behavior of strange particle ratios are different in toward and transverse regions. In the toward region, where auto-correlation bias is absent, the Ω/π shows a mild increasing trend with respect to increase in R_{T}. The Ξ/π and Λ/π, unexpectedly does not show significant dependence on R_{T}. However, in the transverse region, where autocorrelation bias is dominated as R_{T} is defined in the same region, the mild Ω/π enhancement disappears in the ratios of strange mesons to pions. In contrast, the neutral hadrons to pion ratios,
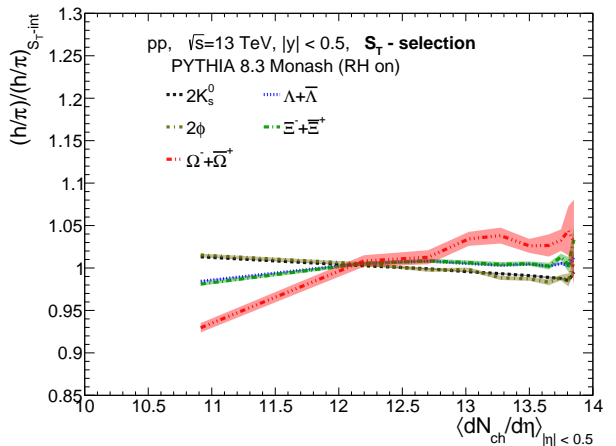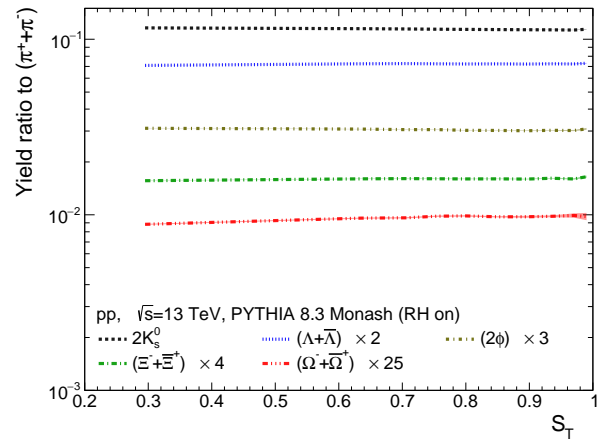

FIG. 10: p_{T}-integrated yield ratios to pions as a function of p_{T}−unweighted transverse sphericity (S_T) (top) and particle yield ratios to pions normalized to the values obtained for the sphericity integrated events (bottom) obtained for $|y| < 0.5$ in pp collisions at $\sqrt{s} = 13$ TeV using PYTHIA 8.

such as ϕ/π, K_S^0/π and Λ/π decrease with an increase in R_{T}. This effect seems to be coming purely from autocorrelation bias. Similar to sphericity and spherocity, the strangeness enhancement feature is also found to be weak in the relative transverse activity classifier. This could be because of the high-p_{T} selection of trigger particle, one always looks at high-multiplicity events, and the multiplicity coverage is similar to spherocity selection, as can be seen in the bottom panels of Fig. 11. The bottom panel shows the strange and multi-strange hadron yield ratios to pions normalized to that for R_{T}-integrated events as a function of $\langle dN_{\text{ch}}/d\eta \rangle$ in different classes of events selected via R_{T} distributions in pp collisions at $\sqrt{s} = 13$ TeV using PYTHIA 8. The double ratio of ϕ, K_S^0 and Λ decrease with increase in $\langle dN_{\text{ch}}/d\eta \rangle$ when the events are selected R_{T} indicating the presence of strong autocorrelation bias.

The charged particle flattenicity dependence of the ratios K_S^0/π, Λ/π, Ξ/π, ϕ/π, and Ω/π is shown in top

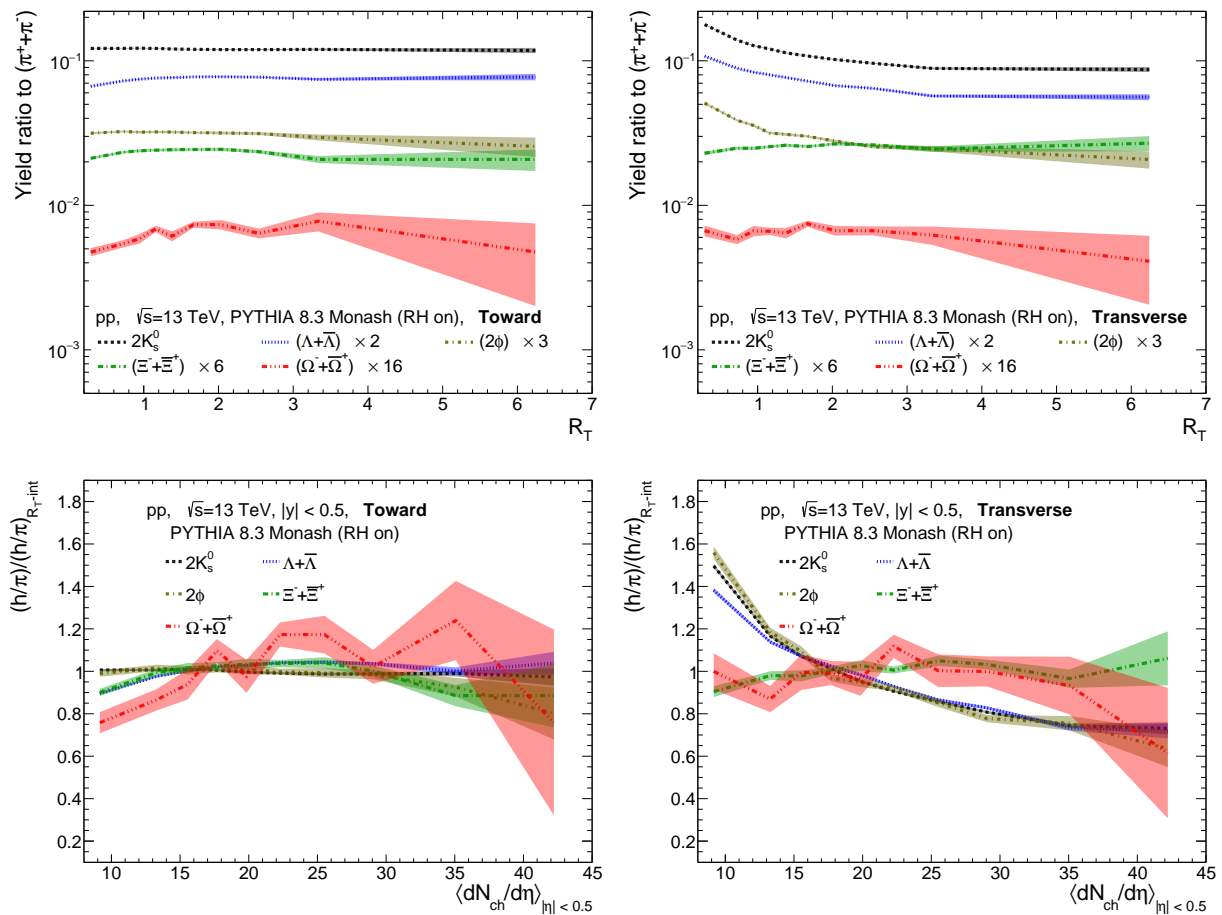FIG. 11: p_{T}-integrated yield ratio to pions (top) and particle yield ratios to pions normalized to the values obtained for the minimum bias event (bottom) obtained in $|y| < 0.5$ as a function of R_{T} in toward (left) and transverse (right) regions of pp collisions at $\sqrt{s} = 13$ TeV using PYTHIA 8.

panel of Fig. 12 for pp collisions at $\sqrt{s} = 13$ TeV using PYTHIA 8. It is interesting to note that these ratios increase as a function of $1-\rho_{\mathrm{ch}}$ for all considered strange and multi-strange hadrons, except for K_S^0. A sudden increase in the slope of the ratios is observed in Fig. 12 for the higher values of $1-\rho_{\mathrm{ch}}$ $(0.75 \lesssim 1-\rho_{\mathrm{ch}} \lesssim 0.95)$ compared to the lower values of $1-\rho_{\mathrm{ch}}$ $(0.35 \lesssim 1-\rho_{\mathrm{ch}} \lesssim 0.75)$. It is found that the rate of increase of the strange to non-strange particle ratios is strange quantum number dependent; the triple-strange baryons such as Ω have more slope compared to the single and double strange baryons such as Ξ, and Λ. In addition, the hidden strange meson, ϕ shows a small dependence on event selection based on $1-\rho_{\mathrm{ch}}$. Here, the values of yield ratios of the multi-strange hadrons to pions for the lowest and highest $1-\rho_{\mathrm{ch}}$ classes are comparable to corresponding classes of N_{mpi} and $N_{\mathrm{ch}}^{\mathrm{fwd}}$ in Figs. 4 and 5, respectively.

The bottom panel of Fig. 12 shows the strange hadron yield ratios to pions scaled to those obtained in flattenicity integrated events as a function of $\langle dN_{\mathrm{ch}}/d\eta \rangle$ obtained in different classes of $(1-\rho_{\mathrm{ch}})$ in pp collisions at $\sqrt{s} = 13$

TeV using PYTHIA 8. Here, one finds that the coverage of $\langle dN_{\mathrm{ch}}/d\eta \rangle$ for highest and lowest classes of (1-ρ_{ch}) is similar to that observed in the lower panel of Fig. 4 using $N_{\mathrm{ch}}^{\mathrm{fwd}}$. In addition, the double ratios for all strange and multi-strange hadrons increase linearly with $\log(\langle dN_{\mathrm{ch}}/d\eta \rangle)$. The rate of increase of the double ratio with $\log(\langle dN_{\mathrm{ch}}/d\eta \rangle)$ is highest for Ω, while the slope decreases and becomes almost zero for K_S^0. The hidden strange, ϕ, lies between K_S^0 and Λ, which is close to the observations in Fig. 5 where events are selected with N_{mpi}. The close resemblance between strange hadron production with N_{mpi} and ρ_{ch} makes charged particle flattenicity one of the ideal choices among the existing event shapes for the study of strangeness production in pp collisions at the LHC.

IV. SUMMARY

We present an extensive summary of the strange particle ratios to pions as a function of different event classi-
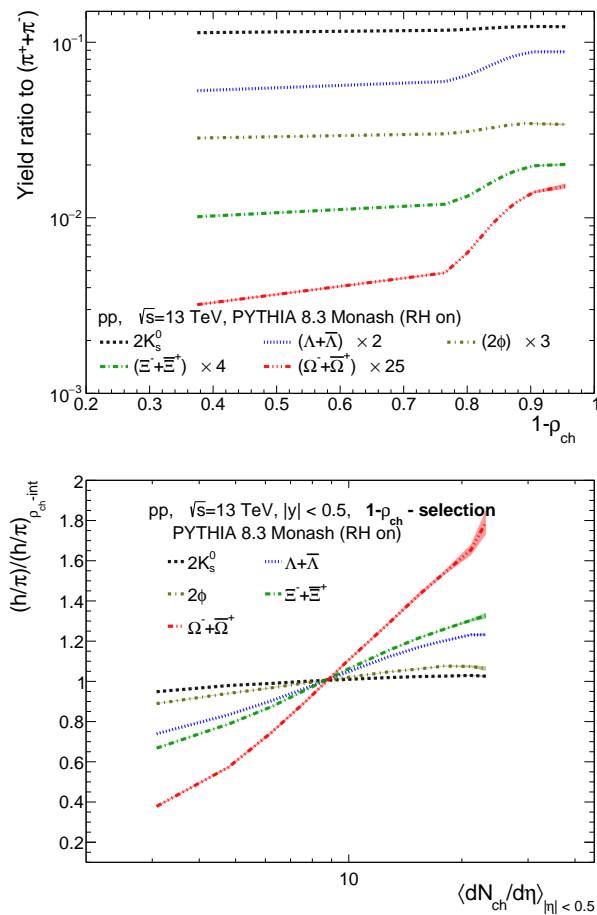
FIG. 12: p_T-integrated yield ratio to pions (top) and particle yield ratios to pions normalized to the values obtained for the minimum bias events (bottom) in $|y| < 0.5$ as a function of charged particle flattenicity (ρ_{ch}) in pp collisions at $\sqrt{s} = 13$ TeV using PYTHIA 8.

fiers using the PYTHIA 8 model with color reconnection and rope hadronization mechanisms to understand the microscopic origin of strangeness enhancement in pp collisions and also prescribe the applicability of these event classifiers in the context of strangeness enhancement. Let us now summarize the conclusions from each event classifier.

- **Number of multi-parton interactions**: MPI plays a pivotal role in particle production, and it is also observed for strange and multi-strange hadrons. A clear strangeness enhancement (suppression) is seen for high (low) multiplicity pp collisions when studied as a function of the number of multi-parton interactions.

- **Charged-particle multiplicity in mid-rapidity**: Multiplicity measured in mid-rapidity shows strangeness enhancement, but the results are significantly prone to autocorrelation bias. The

strangeness suppression in low multiplicity is not seen except for Ω.

- **Charged-particle multiplicity in forward-rapidity**: Multiplicity measured in forward-rapidity significant reduction of autocorrelation bias, but it is prone to a selection bias of choosing high-momentum particles. The model describes the observed strangeness enhancement by the ALICE experiment.

- **Transverse spherocity**: Due to an implicit cut on the minimum number of charged particles being larger than 10, the multiplicity reach for the studies based on spherocity selection is limited towards high-multiplicity. Even at high-multiplicity, the isotropic events show larger enhancement compared to jetty events. The usage of p_T-unweighted definition of spherocity definition results in larger enhancement in high-multiplicity collisions.

- **Transverse sphericity**: A similar behavior of spherocity is seen when studied as a function of transverse sphericity. However, quantitatively the strangeness enhancement is lesser compared to transverse spherocity.

- **Relative transverse activity classifier**: With a high transverse momentum cut for trigger particle, one probes high-multiplicity events with R_T. The studies based on R_T in the transverse region show significant autocorrelation bias while towards the region, which is free from biases, shows mild strangeness enhancement for Ω.

- **Charged-particle flattenicity:** The most recent event shape observable, charged-particle flattenicity, is found to be most suited for the study of strangeness-enhancement and at high multiplicity It shows a similar quantitative enhancement as seen for the study-based on number of multi-parton interactions.

As, significantly higher statistics would be available in Run 3 of the LHC with respect to Run 1 and Run 2, all the above discussed event-classifiers can be experimentally used to probe strangeness with a high level of precision. This manuscript will provide a baseline for such studies and the comparison of experimental results will give a clear insight into the microscopic origin of strangeness enhancement (suppression) in high (low) multiplicity pp collisions at the LHC.

[1] J. Rafelski and B. Muller, Phys. Rev. Lett. **48**, 1066 (1982).

[2] P. Koch, B. Muller and J. Rafelski, Phys. Rept. **142**, 167 (1986).

[3] J. Rafelski, Phys. Lett. B **262**, 333 (1991).

[4] B. B. Abelev *et al.* [ALICE], Phys. Lett. B **728**, 216 (2014). [erratum: Phys. Lett. B **734**, 409 (2014)].

[5] J. Adam *et al.* [ALICE], Nature Phys. **13**, 535 (2017).

[6] V. Khachatryan *et al.* [CMS], JHEP **09**, 091 (2010).

[7] V. Khachatryan *et al.* [CMS], Phys. Lett. B **765**, 193 (2017).

[8] S. Chatrchyan *et al.* [CMS], Eur. Phys. J. C **72**, 2164 (2012).

[9] E. Andersen *et al.* [WA97], Phys. Lett. B **449**, 401 (1999).

[10] F. Antinori *et al.* [NA57], J. Phys. G **37**, 045105 (2010).

[11] F. Antinori *et al.* [NA57], J. Phys. G **32**, 427 (2006).

[12] C. Alt *et al.* [NA49], Phys. Rev. Lett. **94**, 192301 (2005).

[13] C. Alt *et al.* [NA49], Phys. Rev. C **78**, 034918 (2008).

[14] J. Adams *et al.* [STAR], Phys. Rev. Lett. **92**, 182301 (2004).

[15] B. I. Abelev *et al.* [STAR], Phys. Lett. B **673**, 183 (2009).

[16] J. Adams *et al.* [STAR], Phys. Rev. Lett. **98**, 062301 (2007).

[17] B. I. Abelev *et al.* [STAR], Phys. Rev. C **77**, 044908 (2008).

[18] B. B. Abelev *et al.* [ALICE], Phys. Lett. B **728**, 25 (2014).

[19] J. Adam *et al.* [ALICE], Phys. Lett. B **758** , 389 (2016).

[20] S. Acharya *et al.* [ALICE], Phys. Rev. C **99**, 024906 (2019).

[21] S. Acharya *et al.* [ALICE], Eur. Phys. J. C **80**, 693 (2020).

[22] S. Hamieh, K. Redlich and A. Tounsi, Phys. Lett. B **486**, 61 (2000).

[23] K. Redlich and A. Tounsi, Eur. Phys. J. C **24** (2002), 589-594

[24] J. L. Nagle and W. A. Zajc, Ann. Rev. Nucl. Part. Sci. **68**, 211 (2018).

[25] T. Pierog, I. Karpenko, J. M. Katzy, E. Yatsenko and K. Werner, Phys. Rev. C **92**, 034906 (2015).

[26] T. Sjöstrand, S. Ask, J. R. Christiansen, R. Corke, N. Desai, P. Ilten, S. Mrenna, S. Prestel, C. O. Rasmussen and P. Z. Skands, Comput. Phys. Commun. **191**, 159 (2015).

[27] A. Ortiz Velasquez, P. Christiansen, E. Cuautle Flores, I. Maldonado Cervantes and G. Paić, Phys. Rev. Lett. **111**, 042001 (2013).

[28] C. Bierlich, G. Gustafson, L. Lönnblad and A. Tarasov, JHEP **03**, 148 (2015).

[29] C. Bierlich, G. Gustafson and L. Lönnblad, [arXiv:1612.05132 [hep-ph]].

[30] S. Acharya *et al.* [ALICE], Phys. Lett. B **843**, 137649 (2023).

[31] E. Cuautle, R. Jimenez, I. Maldonado, A. Ortiz, G. Paic and E. Perez, arXiv:1404.2372 [hep-ph].

[32] A. Ortiz, G. Paic and E. Cuautle, Nucl. Phys. A **941**, 78 (2015).

[33] A. Khuntia, S. Tripathy, A. Bisht and R. Sahoo, J. Phys. G **48**, 035102 (2021).

[34] A. Banfi, G. P. Salam and G. Zanderighi, JHEP **06**, 038 (2010).

[35] A. Ortiz, Adv. Ser. Direct. High Energy Phys. **29**, 343 (2018).

[36] S. Acharya *et al.* [ALICE], JHEP **05**, 184 (2024).

[37] G. Hanson, G. S. Abrams, A. Boyarski, M. Breidenbach, F. Bulos, W. Chinowsky, G. J. Feldman, C. E. Friedberg, D. Fryberger and G. Goldhaber, *et al.* Phys. Rev. Lett. **35**, 1609 (1975).

[38] B. Abelev *et al.* [ALICE], Eur. Phys. J. C **72**, 2124 (2012).

[39] A. M. Sirunyan *et al.* [CMS], Eur. Phys. J. C **79**, 123 (2019).

[40] T. Martin, P. Skands and S. Farrington, Eur. Phys. J. C **76**, 299 (2016).

[41] G. Bencedi, A. Ortiz and A. Paz, Phys. Rev. D **104**, 016017 (2021).

[42] P. Palni, A. Khuntia and P. Bartalini, Eur. Phys. J. C **80**, 919 (2020).

[43] A. Ortiz and G. Paic, Rev. Mex. Fis. Suppl. **3**, 040911 (2022).

[44] S. Acharya *et al.* [ALICE], arXiv:2407.20037 [hep-ex].

[45] A. Ortiz, A. Khuntia, O. Vázquez-Rueda, S. Tripathy, G. Bencedi, S. Prasad and F. Fan, Phys. Rev. D **107**, 076012 (2023).

[46] C. Bierlich, Nucl. Phys. A **982**, 499 (2019).

[47] C. Flensburg, G. Gustafson and L. Lonnblad, JHEP **08**, 103 (2011).

[48] C. Bierlich and J. R. Christiansen, Phys. Rev. D **92**, 094010 (2015).

[49] C. B. Duncan and P. Kirchgaeßer, Eur. Phys. J. C **79**, 61 (2019).

[50] S. Gieseke, P. Kirchgaeßer and S. Plätzer, Eur. Phys. J. C **78**, 99 (2018).

[51] H. Hushnud and K. Dey, Nucl. Phys. A **1046**, 122868 (2024).

[52] T. Sjostrand, S. Mrenna and P. Z. Skands, Comput. Phys. Commun. **178**, 852 (2008).

[53] PYTHIA 8 online manual: https://pythia.org/latest-manual/Welcome.html.

[54] P. Skands, S. Carrazza and J. Rojo, Eur. Phys. J. C **74**, 3024 (2014).

[55] B. Andersson, G. Gustafson, G. Ingelman and T. Sjostrand, Phys. Rept. **97**, 31 (1983).

[56] J. Adam *et al.* [ALICE], Phys. Lett. B **753**, 319 (2016).

[57] T. Sjostrand and P. Z. Skands, JHEP **03**, 053 (2004).